Use of a FishEye Camera for GNSS NLOS Exclusion and Characterization in Urban Environments

Jan Sanromà Sánchez, Andreas Gehrmann, Paul Thevenon, Philippe Brocard, Amani Ben Afia, Olivier Julien
Ecole Nationale de l'Aviation Civile (ENAC), Toulouse, France

BIOGRAPHIES

Jan Sanromà Sánchez graduated as an aeronautical engineer in 2013 at Universitat Politècnica de Catalunya (UPC), Barcelona, Spain. He then obtained his MSc in Aerospace Science and Technology in 2015. He worked as a research assistant in Signal processing and navigation (SIGNAV) research group at École Nationale de l'Aviation Civile (ENAC) in Toulouse, France. His research focused is on navigation in urban environments and the use of fish-eye camera to increase positioning accuracy.

Andreas Gehrmann graduated from the Technical University of Berlin, Germany, with a Master of Science (MSc) in Electrical Engineering, in 2015. He studied at the Signal Processing and Navigation (SIGNAV) research group at ENAC, in 2014 and 2015. His research focused on positioning in urban areas, using GNSS, INS, and a fish-eye camera for NLOS detection. Since March 2015, he has been working as a software engineer for gas detection systems, at Draeger Saftey AG & Co. KGaA, in Lübeck, Germany.

Dr. Paul Thevenon graduated as electronic engineer from Ecole Centrale de Lille in 2004 and obtained in 2007 a research master at ISAE in space telecommunications. In 2010, he obtained a PhD degree in the signal processing laboratory of ENAC in Toulouse, France. From 2010 to 2013, he was employed by CNES, to supervise GNSS research activities. Since the July 2013, he is employed by ENAC as Assistant Professor. His current activities are GNSS signal processing, GNSS integrity monitoring and hybridization of GNSS with other sensors.

Philippe Brocard is graduated from ENAC (the French civil aviation school) with an engineer diploma in 2012. He is currently a PhD student at ENAC and studies signal processing algorithms, sensor fusion and integrity monitoring techniques adapted to the navigation in urban areas. His thesis is funded by GSA (European GNSS Agency), ENAC and Egis Avia.

Amani Ben Afia graduated in 2012 as an Electronics engineer from ENAC (French National Civil Aviation School), Toulouse, France. Since 2013, she has been a PhD student in the Signal Processing and Navigation Research Group (SIGNAV) of ENAC. Her research focuses on developing multi-sensor fusion algorithms for the navigation in constrained environments.

Dr. Olivier Julien is the head of the Signal Processing and Navigation (SIGNAV) research group of the TELECOM laboratory of ENAC, in Toulouse, France. He received his engineer degree in 2001 in digital communications from ENAC and his PhD in 2005 from the Department of Geomatics Engineering of the University of Calgary, Canada. His research interests are turned towards the use of satellite-based navigation systems for safe navigation.

ABSTRACT

This article presents a new integration method for GNSS, INS and a fish-eye camera for improving vehicle navigation accuracy in urban environments.
In general, the quality of satellite navigation systems in cities tends to be quite poor. The influence of multipath, masking and Non-Line-of-Sight (NLOS) signals can degrade the GNSS position accuracy up to tens of meters, making the solution quite unusable for precise applications. In this article, it is proposed to integrate a wide field-of-view fish-eye camera, mounted on the roof of the car and facing up. This camera is used to detect which satellites are in direct Line-of-Sight (LOS), and which are hidden behind buildings, potentially resulting in NLOS. This camera is integrated together with a GNSS and INS sensors, which will allow a vehicle to navigate in city canyons.
This article first presents the algorithm for GNSS and INS integration using an Extended Kalman filter, as well as the models used for the GNSS measurements. It then presents the NLOS detection method, which mixes the information given by the camera together with the received C/N_0 in order to estimate which satellites are in direct view of the receiver.
The performance of the algorithm is finally tested in the urban environment of Toulouse using ENAC's own test van. The tests show that the GNSS/INS/Fish-eye camera integration does work as a stand-alone device and it allows for a more accurate positioning in urban environments.

INTRODUCTION

Urban environments present a significant challenge for modern Global Navigation Satellite Systems (GNSS)-based systems. These systems were originally designed to work in open outdoor areas, where direct line-of-sight view of the satellite is always possible. In cities however, surrounding buildings block the view of the satellite and their coming signals. The signals from these satellites can however arrive at the receiver trough different reflections, or multipath, still with strength. These reflections cause an increase in the travel distance of the signal, and thus these NLOS signals create large errors in the pseudorange measurements.

A usual solution to this problem is to mix GNSS information together with INS. INS estimate the user's dynamics and provide a position solution without using any external agent, and thus they do not suffer from problems when being used in urban environments. By mixing them with GNSS it is possible to produce a higher accuracy solution, reducing the importance of NLOS and achieving a better navigation solution. The problem of multipath and NLOS is however still present.

What is proposed in this paper is to use a wide field of view (FOV) camera mounted on the roof of a car and looking upward. This camera will take a snapshot synchronized with GNSS measurements. Then, by projecting the satellites on that image, it is intended to determine which satellites are in the section of visible sky, and which are hidden behind buildings and sending NLOS signals. All the sensors used will represent cheap, mass market devices, in order to show the performance of a generic configuration.

The main objective is thus to develop an algorithm that is capable to analyze each picture and detect which satellites are NLOS. Those satellites can then be removed from the computation, ideally eliminating the effect of multipath. By combining INS and camera exclusion with the GNSS measurements, a higher accuracy and more robust solution should be achieved.

GNSS/INS INTEGRATION

In this section the integrated INS/GNSS architecture is presented. Sensor fusion will allow combining the benefits of both GNSS and INS, and achieve a high level of accuracy and availability in urban environments.

The integration algorithm uses a tightly coupled integration scheme based on a Kalman filter as presented in [1]. The general strategy of a tightly-coupled architecture is to use GNSS measurements (pseudorange and Doppler) in order to produce an estimate of the inertial navigation system errors. These errors are mainly due to the inertial measurement unit (IMU) biases. Once estimated, these biases can be feedback to the IMU in a closed-loop correction. Figure 1 shows the general scheme of the proposed integration algorithm.

In this architecture, the inertial navigation system estimates the vehicle position, velocity and attitude using the IMU measurements. This navigation solution is input to the Kalman filter which estimates, in addition to the IMU biases, the errors of this inertial solution using GNSS pseudoranges and Doppler measurements and outputs the corrected navigation solution.

GNSS measurement models

Pseudoranges and Doppler measurements were used in the Kalman filter. Both types must thus be correctly modeled in order to properly tune the Kalman filter.

The pseudorange measurement is an estimate of the distance between the GNSS satellite and the receiver antenna, but also includes the mis-synchronization of satellite and receiver local oscillators. This measurement is computed from the propagation time between the transmission of the signal by the satellite and its reception by the receiver, and the multiplication of this time by the speed of light *c*. The fact that the clocks of the satellites and the receiver are not perfectly synchronized to GPS time, introduces a clock bias that drifts with time. Therefore, the pseudorange (PR) measurement can be modeled as:

$$\tilde{\rho}_G^i = r^i + c\delta t + \eta_{\rho G}^i \quad (1)$$

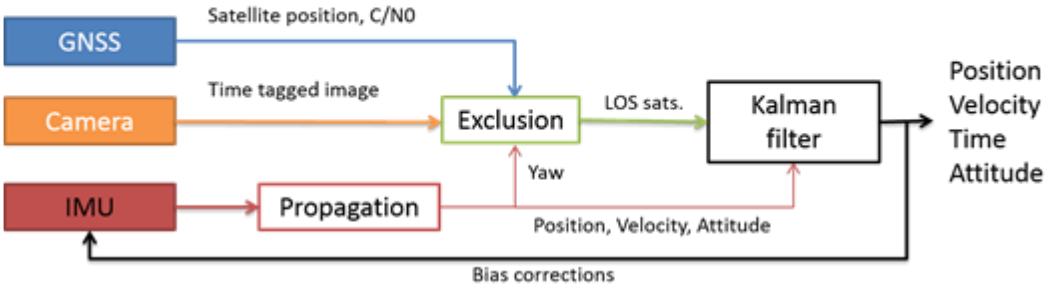

Figure 1: Integration scheme between GNSS, INS and camera exclusion

where

- r^i is the true range between the satellite *i* and the receiver antenna,
- δt is the clock bias and
- $\eta^i_{\rho G}$ is a zero-mean white Gaussian noise with a variance denoted by σ^2_{PR}

The Doppler measurement represents the rate of change of the carrier phase. The multiplication of this measurement by the signal wavelength λ provides the pseudorange rate (PRR) measurement:

$$\dot{\rho}^i_G = \tilde{d}^i_G \lambda = \dot{r}^i + c\dot{\delta}t + \eta^i_{\dot{\rho}G} \quad (2)$$

where

- $\tilde{d}^i_G$ is the Doppler measurement of satellite *i*,
- $\dot{r}^i$ is the true pseudorange rate between the satellite and the receiver,
- $\dot{\delta}t$ is the clock drift and
- $\eta^i_{\dot{\rho}G}$ is the range rate error modeled as a zero-mean Gaussian white noise with a variance denoted by σ^2_{PRR}.

In cities, the biggest source of measurement errors will be the local effects affecting the tracking loops, on top of which will be multipath- and NLOS-induced errors. In order to try to correctly model this type of errors for both the pseudorange and pseudorange rate, the models proposed in [2] and [3], based on data collection in urban environments and commercial mass market receivers, were used. These models were specially proposed for use in urban environments, under conditions of heavy multipath.

For the pseudorange measurements, the covariance of the measurements' errors is defined as a function of the C/N_0 as:

$$\sigma^2_{PR} = a + b10^{\frac{-C/N_0}{10}} \quad (3)$$

Parameters a and b of (3) are defined as in Table 1.

Table 1: Parameters for Pseudorange Error Variance

Measurement	a	b
Pseudorange	-1.5	731^2

For the Doppler measurements, this variance is defined as a function of the user velocity and received C/N_0 according to "the Doppler measurement standard deviation as a function of velocity and C/N_0" table defined in [2].

Inertial Measurements Models

When fusing the data from GNSS and an INS, the position, velocity and attitude are predicted with the INS. Therefore, the Kalman filter process model shall characterize the evolution of the error on the states as propagated with the INS. These error models can be derived from the inertial sensors error models. The error sources that affect inertial sensors are classified into biases, scale factors, misalignment and random noise errors. In this paper, the measurement errors of the gyroscopes and accelerometers are modelled as the sum of a noise term which is assumed to be a white Gaussian noise (denoted w_a and w_g), and an in-run bias which is modelled as a first order Gauss-Markov process (denoted b_a and b_g) :

$$\tilde{f}^b_{ib} - f^b_{ib} = b_a + w_a \quad (4)$$

where

- $\tilde{f}^b_{ib}$ is the specific force as measured by the accelerometers and
- f^b_{ib} is the actual specific force

$$\tilde{\omega}^b_{ib} - \omega^b_{ib} = b_g + w_g \quad (5)$$

where

- $\tilde{\omega}\tilde{\omega}^b_{ib}$ is the angular rate as measured by the gyroscopes and
- ω^b_{ib} is the actual angular rate

A medium-cost 6 axis MEMS IMU (Xsens MTi) has been used in this paper. The standard deviation of the noise term and the driven noise of the sensors biases have been derived by analysing the Allan Variance and correlation function of the raw inertial sensors measurements. The results of this study are summarized in Table 2. Moreover, the correlation time for the Gauss-Markov processes has been set to 1000 s for the gyroscopes and 2000 s for the accelerometers.

Table 2: Parameters for the inertial measurements error model

		acc $[\frac{m}{s^2\sqrt{Hz}}]$	gyro $[\frac{^\circ}{h\sqrt{Hz}}]$
bias stability root PSD	x	1.3e-5	1.3
	y	4.7 e-5	
	z	9.5e-6	
Noise root PSD			200

GNSS/INS Integrated Kalman Filter

Based on the integration scheme and the sensors' measurement models previously described, the Kalman state vector can be written in the Earth-Centered-Earth-Fixed (ECEF) frame as:

$$\boldsymbol{X}^e = \left[\delta\boldsymbol{\psi}_{be} \quad \delta\boldsymbol{v}^e \quad \delta\boldsymbol{p}^e \quad \boldsymbol{b}_a \quad \boldsymbol{b}_g \quad c\delta t \quad c\dot{\delta}t\right]^T \quad (6)$$

where

- $\delta\boldsymbol{\psi}_{be}$ is the inertial attitude (orientation of the vehicle body frame (b) with respect to the ECEF (e) frame) error
- $\delta\boldsymbol{v}^e$ is the vehicle velocity error expressed in the (e) frame
- $\delta\boldsymbol{p}^e$ is the vehicle position error in the (e) frame
- $\boldsymbol{b}_a$ and $\boldsymbol{b}_g$ are respectively the IMU accelerometer and gyroscope biases
- $c\delta t$ and $c\dot{\delta}t$ are respectively the GNSS clock bias and clock drift. If multiple GNSSs are used, then the time difference between the two systems should be also estimated in the state-vector. However, the clock drift between the two systems

could be neglected, since GNSS time is very stable.

The Kalman filter propagation step is based on the computation of the navigation solution using the inertial system. The state transition model of the Kalman filter is derived by computing the state-vector rate of change and expressing it as a function of the state-vector and the system noise generated by the IMU and GNSS clock noises. This state transition equation is written as:

$$\dot{\boldsymbol{X}}^e = \boldsymbol{F}^e \boldsymbol{X}^e + \boldsymbol{G}^e \boldsymbol{u} \qquad (7)$$

where

- $\boldsymbol{F}^e$ is the state transition matrix,
- $\boldsymbol{G}^e$ is the system noise distribution matrix and
- $\boldsymbol{u}$ is the covariance of the system noise vector

The expressions of all these matrices and vectors are given in [1].

The Kalman filter update uses the GNSS pseudoranges and pseudorange rate measurements in order to correct the inertial system outputs as well as the IMU biases. The observation model relates the GNSS measurement innovation $\delta \boldsymbol{z}_G$ to the state-vector $\boldsymbol{X}^e$ as follows

$$\delta \boldsymbol{z}_G = \begin{bmatrix} \tilde{\rho}_G^1 - \hat{\rho}_G^1 \\ \vdots \\ \tilde{\rho}_G^N - \hat{\rho}_G^N \\ \tilde{\dot{\rho}}_G^1 - \hat{\dot{\rho}}_G^1 \\ \vdots \\ \tilde{\dot{\rho}}_G^N - \hat{\dot{\rho}}_G^N \end{bmatrix} = \boldsymbol{H}^e \boldsymbol{X}^e + \begin{bmatrix} \eta_{\rho G}^1 \\ \vdots \\ \eta_{\rho G}^N \\ \eta_{\dot{\rho} G}^1 \\ \vdots \\ \eta_{\dot{\rho} G}^N \end{bmatrix} \qquad (8)$$

where

- $\tilde{\rho}_G^i$ is the i[th] satellite measured pseudorange
- $\hat{\rho}_G^i$ is the i[th] satellite pseudorange predicted from the inertial navigation solution
- $\tilde{\dot{\rho}}_G^i$ is the i[th] satellite measured pseudorange rate
- $\hat{\dot{\rho}}_G^i$ is the i[th] satellite pseudorange rate predicted from the inertial navigation solution
- $\boldsymbol{H}^e$ is the measurement matrix. Its expression can be found in [1]

NLOS DETECTION ALGORITHM

By joining INS and GNSS information in a tight architecture, the inertial sensors would guide the solution on those situations where very few GNSS satellites are in view, while GNSS satellites correct the drift present in the INS solution.

While navigating through a city, however, GNSS measurements will be heavily affected by multipath and NLOS satellites. This multipath can cause large errors on the GNSS pseudoranges and Doppler measurements. If these faulty GNSS measurements are not good enough to be used to correct for the INS drift, over time the position accuracy worsens considerably, as errors in the IMU start accumulating in the solution.

As explained before, the worse impact of multipath happens when direct view of the transmitting satellite is blocked by a solid object, like a building. In this situation, the receiver could start tracking a reflected signal coming from the same satellite as the original one. It is with the objective to block multipath, that this paper proposes the use of a high field-of-view (185 °) fish-eye camera.

This camera takes pictures of the sky above (Figure 2), synchronized with the GNSS measurements. It is then possible to compute the satellite elevation and azimuth (which comes from the GNSS ephemeris and approximate receiver location) to project those satellites on the image, as long as the attitude of the camera, provided by the INS, is well estimated. The satellites that are placed in the sky part of the image (in green) can thus be treated as LOS with confidence. Those satellites placed behind a building or any other obstructing object will be considered as NLOS, or at least as less trustworthy signals.

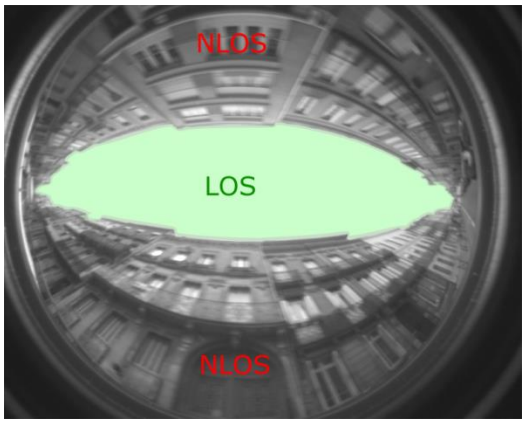

Figure 2: Principle of NLOS exclusion and sky detection (green area).

Once the distinction between LOS and NLOS (or suspicious) signals is made, it is possible to exclude or down-weight the corresponding pseudorange and Doppler measurements in the Kalman filter. This would ideally allow obtaining a better position and attitude solution.

Image Processing Algorithm Description

The objective of the image processing is to tell apart the sky from the surrounding masking buildings in each image. The following operations are applied to an image to perform the identification of the sky vs blocked areas.

1) Morphological closing operation: This operation clears the image of small details like cables or lamp posts that would affect the image segmentation.

2) Canny segmentation: This function [4] detects the edges present in the image. Edges are detected in high-gradient regions of the image. The output is a binary image, in which the white zones represent the edges.

3) Hough line detection: This function looks for line patterns in the image, based on a test checking if different edge pixels follow a geometrical constraint described by the equation of a line [5]. It connects a set of edge points if

they are aligned, allowing to close gaps left by the Canny segmentation.

4) Morphological opening operation: This operation further homogenizes the segmented image, by removing small holes in the image introduced by image noise.

5) Floodfill operation: The floodfill operation changes the color of a certain region to black until an edge is found. As described later, the starting point of the floodfill operation is a satellite perceived as a LOS signal. The filled area will correspond to open sky (LOS), while the unfilled area will correspond to blocked (NLOS) areas.

Mistakes in the image processing can cause NLOS satellites to be used, or LOS satellites to be discarded. Different environments and weather conditions will present different challenges for the image processing and the camera, as they have a great effect on the way the image is captured and its quality. Some of them are:

- **Sun glares, clouds and trees.** These three factors are very limiting in image segmentation as they appear as a solid object in an image. As they have edges in the picture, they limit sky detection, even though they have no effect on pseudorange measurements.
- **Rain:** Although not tested, as the camera is not insulated against water, rain would cause a huge problem as water droplets would block the image. Some hydrophobic spray could be used, and then then the images would only show a cloudy day.
- **Night and tunnels:** Image processing is impossible during night time, as the image cannot properly detect the edge between a building and the sky. Long bridges and tunnels would present a similar problem, with the added problem that fast changes in brightness (like lamps) would blind the camera for a few seconds.

Satellite Selection based on C/N_0

In order to compensate for these problems, the proposed NLOS detection algorithm also uses C/N_0 measurements. It is known that high elevation satellites should have a high C/N_0, while NLOS satellites should have a lower received C/N_0, although NLOS with high C/N_0 can occurr. This information can then be used to make a first estimation of where the visible sky area is in the picture. The overview of the algorithm is as follows:

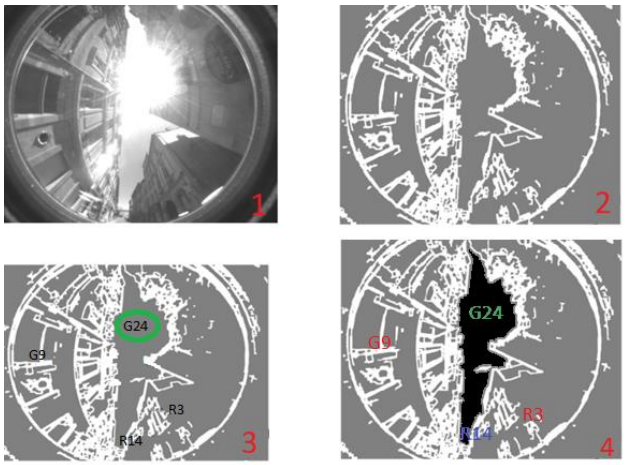

Figure 3: Overview of the exclusion algorithm.

According to

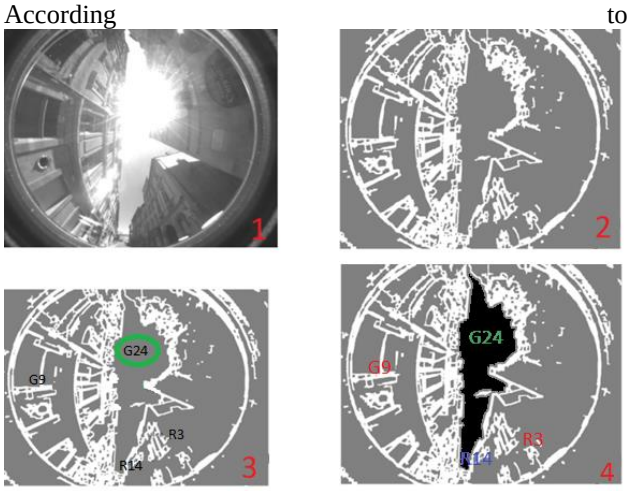

Figure 3:

1) **Original image:** Accurately timed to know its corresponding GNSS and IMU epoch.
2) **Segmented image:** We find the edges in the image to segment it into different zones.
3) Compute the **satellite projection** and project them on the image based on the estimated attitude of the camera given by the IMU.
4) Choose the satellites with a C/N_0 above 45 $dBHz$ (marked in green). Do a **flood fill** starting from these satellites. This operation spreads color until a border is found. Sky is then detected as the black region, and any other satellite present in it will be detected as LOS.

Once the sky area has been detected, it is possible to decide whether the rest of the satellites are LOS or NLOS based on the picture information: if they fall in the dark area (representing the sky) they are considered as LOS, if not they are discarded. In order to avoid the biggest errors, and based on experience, satellites with C/N_0 above 40 $dBHz$ will be automatically considered as LOS, while those with

power levels below 30 $dBHz$ will be considered as NLOS. The different thresholds used can be seen in Figure 4. This is similar to what is proposed in [10].

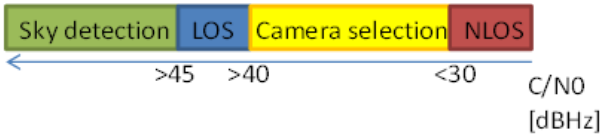

Figure 4: Thresholds for the camera algorithm.

The result of this algorithm is that the camera can be used in the variety of environments described before.

- Clouds or sun glares do not affect the output even though they are detected as edges in the image.
- Trees have a higher effect, as they reduce the C/N_0 measurements a bit, but still they would not fully block the detection.
- In places where no satellites are above the sky detection or LOS thresholds, all satellites are excluded, trusting only the inertial output. This allows the method to be used in tunnels, as any GNSS value received (if any) will be erroneous.
- During night time the C/N_0 will be the same, but the camera information will be useless (another type of camera can be used).

As per processing time, this algorithm runs close to real-time, even though it has only been tested in post processing. This allows fast testing for each of the thresholds and the algorithm accuracy.

TESTS

Test campaign and conditions

Two test campaigns were performed on the same day to show the performance of the NLOS exclusion. One campaign consisted of a mix of suburban and urban environments and lasted for around 40 minutes. The second test included a highway section and lasted 30 minutes. The routes are shown in Figure 5. Toulouse city center consists of very narrow streets with very short houses, just three or four story high. It is worth mentioning also that the day was very sunny and the test was done soon after midday in the summer. It was seen that the sun would blind the camera, making segmentation much more difficult. A significant sun glare can also be seen in the center of most of the images.

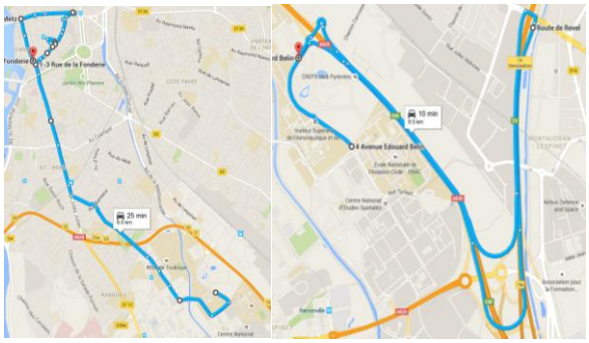

Figure 5: Route to Toulouse centre-ville (left). Highway route (right)

Equipment Set Up

The equipment used consists of cheap to mid-cost sensors with normal mass-market performance:

- U-Blox M8T: GPS/GLONASS receiver. Also used for timing the IMU and camera measurements.
- Xsens MTi IMU
- IDS uEye black and white camera with a fish-eye lens.
- Novatel Span: reference equipment used to evaluate accuracy. [6]

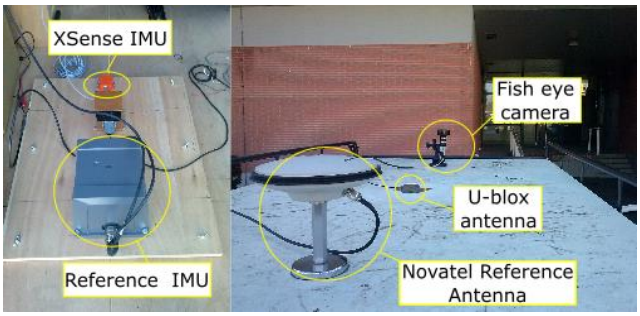

Figure 6: Equipment mounted inside (Left) and on top (right) of a van.

All this equipment was mounted on top of a van for the data collection. The u-Blox receiver being a dual constellation mono-frequency GPS/GLONASS receiver, the increase in satellite availability caused by the dual constellation showed that at least one or two satellites were always in direct LOS view, even in the narrowest streets.
The receiver was also used as a timing reference for the IMU and the camera, which do not include accurate clocks of their own. Pictures and GNSS measurements were taken at 1 Hz, while the IMU has an output rate of 100 Hz.

The reference equipment produced centimeter level positioning and it was used to estimate the positioning accuracy of our algorithm.
The heading estimation used to project the satellites on top of the camera image was initially based on the reference equipment, in order to first only test the selection algorithm

based on the correct projection of the satellites on the image.

Initial Considerations on Code and Doppler Measurements' Filtering

The Kalman Filter innovation gives an indication on the discrepancy between reconstructed GNSS measurements based on the propagated solution and the GNSS measurements. If a large (abnormal) innovation is seen, it can be assumed that it comes from a faulty GNSS measurement, caused by a NLOS satellite. Innovation filtering then consists in setting a threshold, over which one of the measurements is considered as faulty. Table 3 shows the accuracy obtained when adding Doppler innovation filtering with 2 thresholds $4m/s$ and $1m/s$ (user velocity). In this initial test, the camera was not used. It can be seen that Doppler innovation filtering brings a significant improvement in the position accuracy. These results indicate us that Doppler measurements can be extremely untrustworthy in urban environments, although when correctly filtered, they improve the accuracy.

As a consequence, in the forthcoming results, a specific Doppler innovation filtering test is used with threshold of $4m/s$.

Table 3 : Test with Doppler measurement selection in urban environment

Parameters	Integration with Doppler	$4m/s$ max innovation	$1m/s$ max innovation
Mean Horizontal Error [m]	8.43	5.92	3.33
95% Horizontal Error [m]	20.90	14.43	7.84
Max. Horizontal Error [m]	33.29	23.74	23.40
Mean Yaw Error [deg]	7.79	5.26	2.79
95% Yaw Error [deg]	24.78	12.72	6.77
Max Yaw Error [deg]	40.10	19.67	14.26

Besides, initial test using the camera exclusion detection were performed and a parametric analysis was made. In particular, a trade-off between a full exclusion and a simple down-weighting of the NLOS detected measurements was performed. It was shown that an optimal solution (with respect to the test campaign) was to fully exclude all the Doppler measurements from NLOS detected measurements and to only down-weight, by a factor of 1.5 on the variance values, the NLOS-detected pseudorange measurements. This is thus used in the following.

Urban Test

During the urban test, the influence of the camera can be clearly seen. The first 10 minutes of data are located in a suburban area between ENAC and Toulouse center, while the rest was located in the narrow streets of the city center. Table 4 shows the accuracy results for three cases:

- The first one is the case when only the INS/GNSS algorithm is used (no camera exclusion).
- The second column represents the accuracy results when we turn on the camera for NLOS exclusion, and we use the extremely accurate reference heading to project the satellites on the images. This is obviously outside the scope of the system, as it relies on the very expensive reference receiver. Nonetheless it offers a good approximation on how good the NLOS exclusion algorithm is, as there are no errors when projecting the satellites on the image.
- The final column represents what happens when, instead of using the reference heading for projecting the satellites, we use our own estimated heading using our IMU. This would be the performance if we used our GNSS, IMU and camera in an integrated, stand-alone device.

Table 4: accuracy results in the urban environment.

Configuration	INS/GNSS No camera	Camera with Reference heading	Camera with Estimated heading
Mean Horizontal Error [m]	4.24	3.74	3.81
95% Horizontal Error [m]	10.60	8.96	9.63
Max. Horizontal Error [m]	18.67	21.34	22.17
Mean heading Error [°]	3.95	2.55	3.71
95% heading Error [°]	10.11	7.45	8.40
Max heading Error [°]	18.671	11.52	15.13

It can be seen that the NLOS exclusion when using the reference heading does reduce the horizontal error. Both the mean error, and the 95^{th} percentile see a reduction of around one meter when the camera is activated.

Figure 7 and Figure 8 show this tendency over the duration of the test. It can be seen that use of the camera exclusion reduces much of the errors present in the INS/GNSS integration. The heading error, which suffers a lot from the lack of satellite visibility in cities, also decreases to a very usable level.

However, it is worth noting that the maximum horizontal error does increase when using the camera. This is caused by NLOS detection errors in very low visibility areas. These errors cause a decrease in horizontal accuracy for an epoch or two, but then the solution improves again.

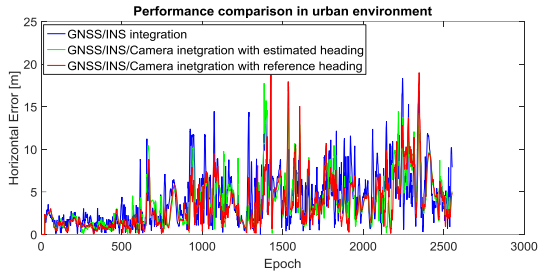

Figure 7: Comparison of horizontal accuracies when using the estimated heading in urban environment.

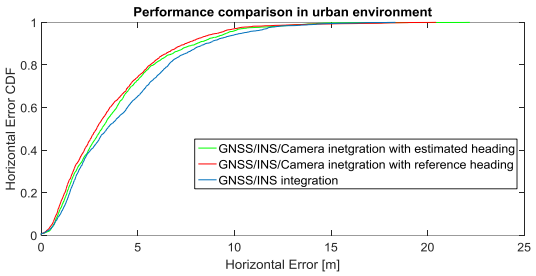

Figure 8: Comparison between the cumulative distribution function of the horizontal error.

In terms of the number of satellites excluded, Figure 9 shows a huge drop in the number of satellites used when the NLOS detection algorithm is used. The mean number of satellites seen by both configurations shows a difference of more than 7 satellites in Toulouse city center (from 15 to less than 8), and about 4 to 5 in sub-urban areas, showing how strong this exclusion is in an urban environment. In the narrowest streets, it can be seen that most of the time there are less than 4 satellites available when using the camera, when more than 10 satellites are generally available.

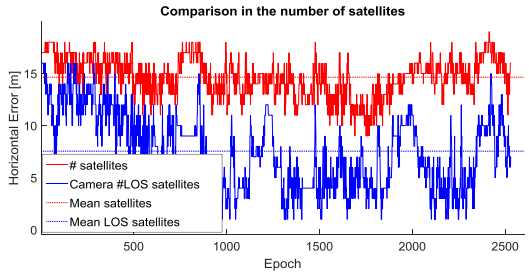

Figure 9: Number of LOS satellites as detected by the camera

Highway test

During the highway test, satellite visibility was much higher, as there were fewer obstacles along the way. Figure 10 shows the decrease in the number of available satellites when using the camera. The graph shows that most of the time only two or three satellites are excluded. However, there are many local drops in the number of satellites. These drops have many causes: bridges and traffic signs overhead would block the view of the camera, and so very few satellites would be used. Trucks driving next to the car would also block the visibility on one side.

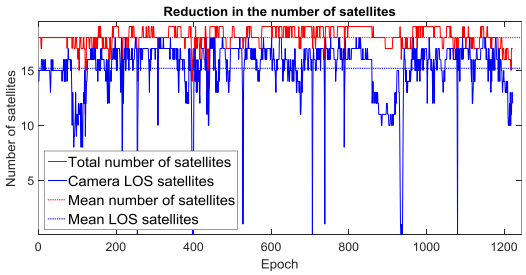

Figure 10: Number of satellites in the highway environment.

The camera then does not add much to the solution accuracy, as seen in Table 5. However some special environments could also be observed in the test. The performance of the algorithm was tested when driving under a short bridge. Figure 11 shows that once inside a tunnel, the algorithm decides (based on C/N0 values) that the van is no longer under open sky (no black areas in the image), and so it discard all satellites (seen in red). It then goes to fully inertial navigation for the duration of the tunnel.

Table 5: Accuracy results in the highway environment.

Configuration	**INS/GNSS No camera**	**Camera with Reference heading**	**Camera with Estimated heading**
Mean Horizontal Error [m]	1.17	1.16	1.18
95% Horizontal Error [m]	2.33	2.21	2.25
Max. Horizontal Error [m]	5.09	7.03	4.55
Mean heading Error [°]	3.78	3.21	3.45
95% heading Error [°]	17.69	17.08	17.08
Max heading Error [°]	39.30	26.90	29.09

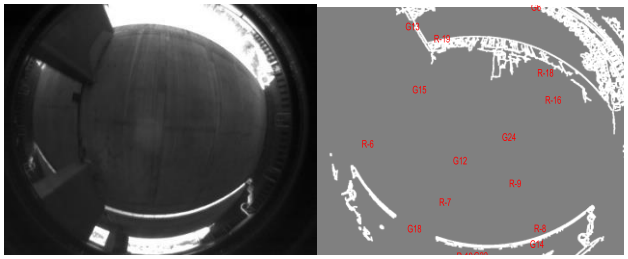

Figure 11: Inside a tunnel. Left: original Image. Right: Processed image.

Figure 12 also shows the performance of the sky detection under trees. Trees cause troubles for the camera exclusion, as they are detected as solid objects in the picture: they have many edges and different colors than the sky, and thus they limit the image segmentation. Since the C/N_0 information is used for the image floodfill, the algorithm knows that those satellites behind the tree are in fact LOS, as their C/N_0 is high. However, many satellites are still detected as NLOS, as the dense foliage does have an effect over the received power levels. One solution could be to interpret such a fragmented image in a specific way associated to the presence of a tree.

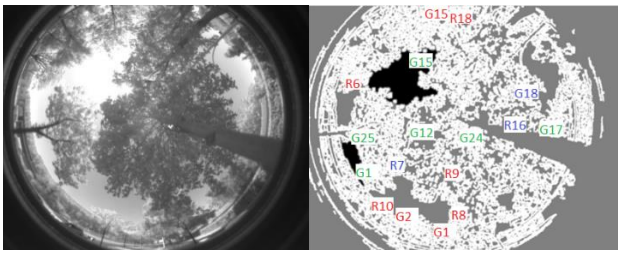

Figure 12: Performance under trees.
Left: original Image.
Right: Processed image. NLOS satellites are in red.

Figure 13 shows how satellites above 40 dB-Hz are always taken as LOS, while satellites with received power below 30 $dBHz$ are taken as NLOS. A gray area exists then between $30 - 40$ $dBHz$ in which the camera performs the main part of its detection works.

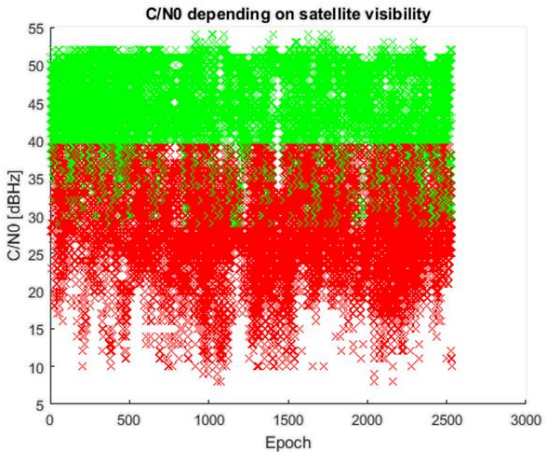

Figure 13: C/N_0 depending on visibility. Green represents LOS and red NLOS.

CONCLUSIONS AND FUTURE WORK

This article has shown an algorithm in which INS, GNSS and fisheye camera data are integrated in order to produce accurate positioning in urban environments. The tests performed with the algorithm show that it is a viable option, and that it does increase the accuracy of the solution. This increase in accuracy happens with respect to a GNSS/INS solution which is already quite precise, as the use of double constellation already allows for very good positioning.

The most important factor in these results is that the integration was proved to work as a stand-alone device. The u-Blox receiver can be used together with the xSense IMU and the IDS fish-eye camera in order to produce a more accurate solution for urban environments.

It is also important to mention the fact that the test route was in no way thought or planned to prove any performance. The route included the normal characteristics of urban environments and the weather conditions were not especially favorable for the camera detection, as the camera would be blinded by the sun.

Future work on this subject is still necessary, as the increase of accuracy does not necessarily justify the cost of adding a camera into the integration. Three main areas of quick improvement are seen for the current status of the integration algorithm:

- fine tuning of the thresholds used for the NLOS exclusion, as seen in Figure 4. The current threshold was not based on hard data of the receiver's performance. The thresholds could probably be raised in order to obtain a more robust and accurate solution.
- use of a color camera instead of a black and white one. The increased quality and range of colors will make segmentation between sky and buildings much easier, reducing the errors.

Finally, it is worth mentioning that such an equipment could be used to evaluate the NLOS measurements

characteristics. Indeed, most of the safety-critical applications that are using GNSS-based location devices working in urban or sub-urban environments required a knowledge on the NLOS occurrence rate and NLOS measurement error distribution. The proposed scheme is fully able to do so since it can be integrated with a reference trajectory system. Therefore, measurement errors can be accurately estimated and can be associated to LOS and/or NLOS situations. It can also be related to the satellite elevation and/or azimuth. Initiating such measurement campaigns is thus also part of the future work.

REFERENCES

[1] P. D. Groves, Principles of GNSS, inertial, and multisensor integrated navigation systems, London: Artech House, 2013.

[2] S. Carcanague, "Low-cost GPS/GLONASS Precise Positioning Algorithm in Constrainted Environments," Universite de Toulouse, Toulouse, France, 2013.

[3] H. Kuusniemi, "User level reliability and quality monitoring in satellite based personal," Tampere University of Technology, Tampere, Finland, 2005.

[4] J. Canny, "A Computation Approach to Edge Detection," *IEEE Transactions on Pattern Analysis and Image Understanding*, vol. 18, no. 6, 1986.

[5] C. Galambos, J. Kittler and J. Matas, "Gradient-based Progressive Probabilistic Hough Transform," *IEE Vision Image and Signal Processing*, vol. 148, no. 3, pp. 158-165, 2002.

[6] Novatel, "proPak6," [Online]. Available: http://www.novatel.com/products/span-gnss-inertial-systems/span-receivers/span-enclosures/span-on-propak6/.

[7] "uEye camera specifications," IDS, [Online]. Available: https://en.ids-imaging.com/video_ueye.html. [Accessed 2014].

[8] "Fujinon Fish-eye specification," Fujifilm, [Online]. Available: http://www.fujifilmusa.com/products/optical_devices/security/fish-eye/5-mp/fe185c057ha-1/. [Accessed July 2015].

[9] A. Gehrman, "Positioning in Urban areas," Master Thesis report, STU Berlin, Berlin, 2014.

[10] N. K. Taro Suzuki, "N-LOS GNSS Signal Detection Using Fish-eye camera for vehicle navigation in urban environments," *ION GNSS+* , 2014.